PNAS
www.pnas.org

Supplementary Information for

Stormier Southern Hemisphere induced by topography and ocean circulation

Tiffany A. Shaw, Osamu Miyawaki and Aaron Donohoe

Corresponding Author name.
E-mail: tas1@uchicago.edu

This PDF file includes:

Figs. S1 to S11 (not allowed for Brief Reports)
Tables S1 to S3 (not allowed for Brief Reports)

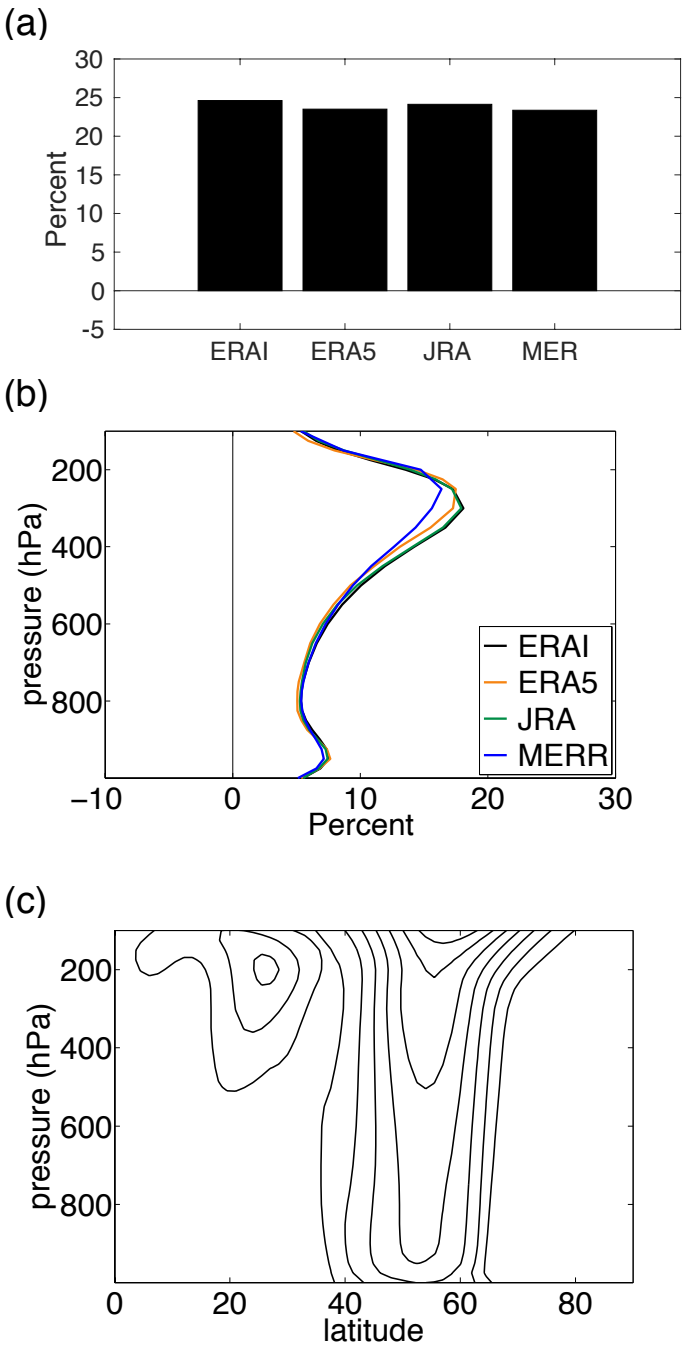

Fig. S1. Difference of Southern and Northern Hemisphere storminess measured by transient eddy kinetic energy (a) vertically integrated, longitudinally-mean and averaged poleward of 20°, (b) vertically-varying storminess averaged poleward of 20° and divided by the value at 250 hPa in the Northern Hemisphere and (c) longitudinal-mean zonal wind (2 ms^{-1} contour interval) averaged over reanalysis data sets.

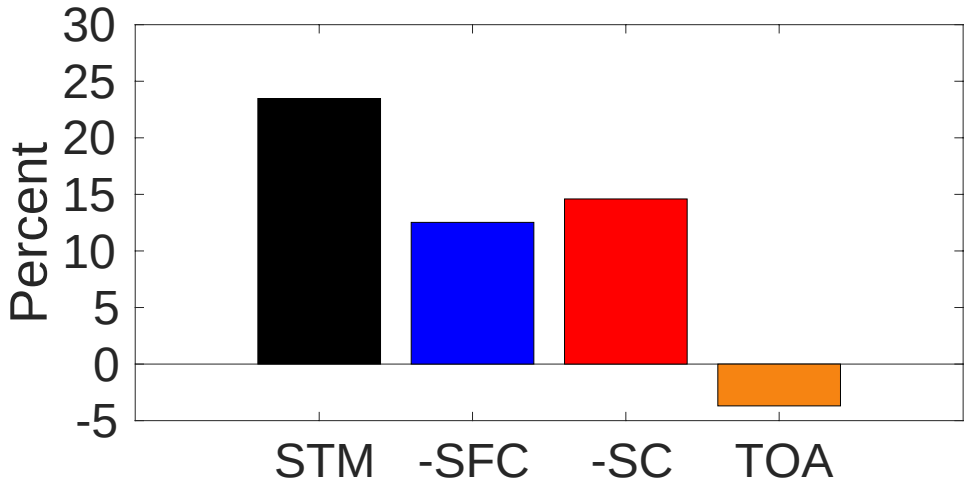

Fig. S2. Percentage difference of present-day rescaled energetic storminess (difference of Southern and Northern Hemisphere divided by Northern Hemisphere) in ERA5 data from 1980 to 2018 for longitudinal-mean, vertically-integrated, latitudinally-integrated (poleward of 20°) transient eddy moist static energy flux (STM) decomposed into surface energy flux (SFC), stationary circulation (SC) and top-of-atmosphere (TOA) contributions.

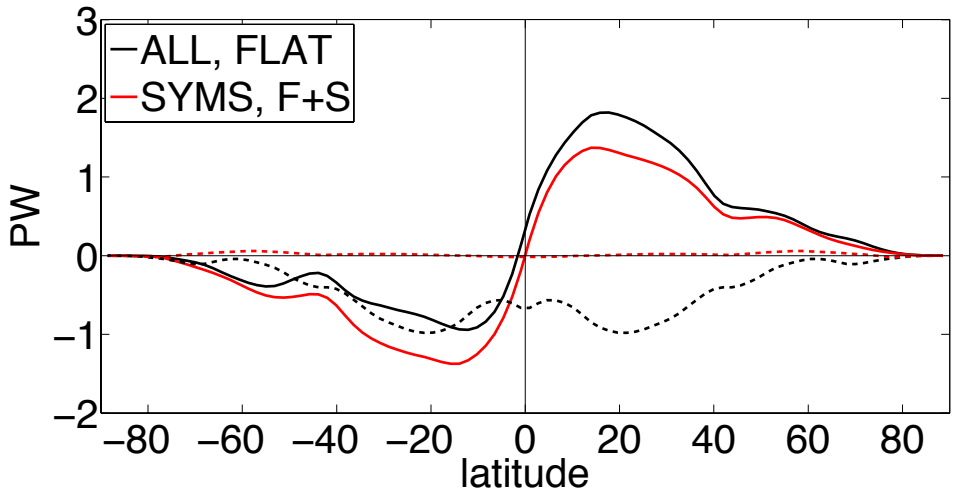

Fig. S3. Ocean energy transport inferred from observationally-estimate surface energy fluxes imposed in ECHAM6 climate model simulations (solid lines) and hemispheric asymmetry (Southern Hemisphere minus Northern Hemisphere, dashed).

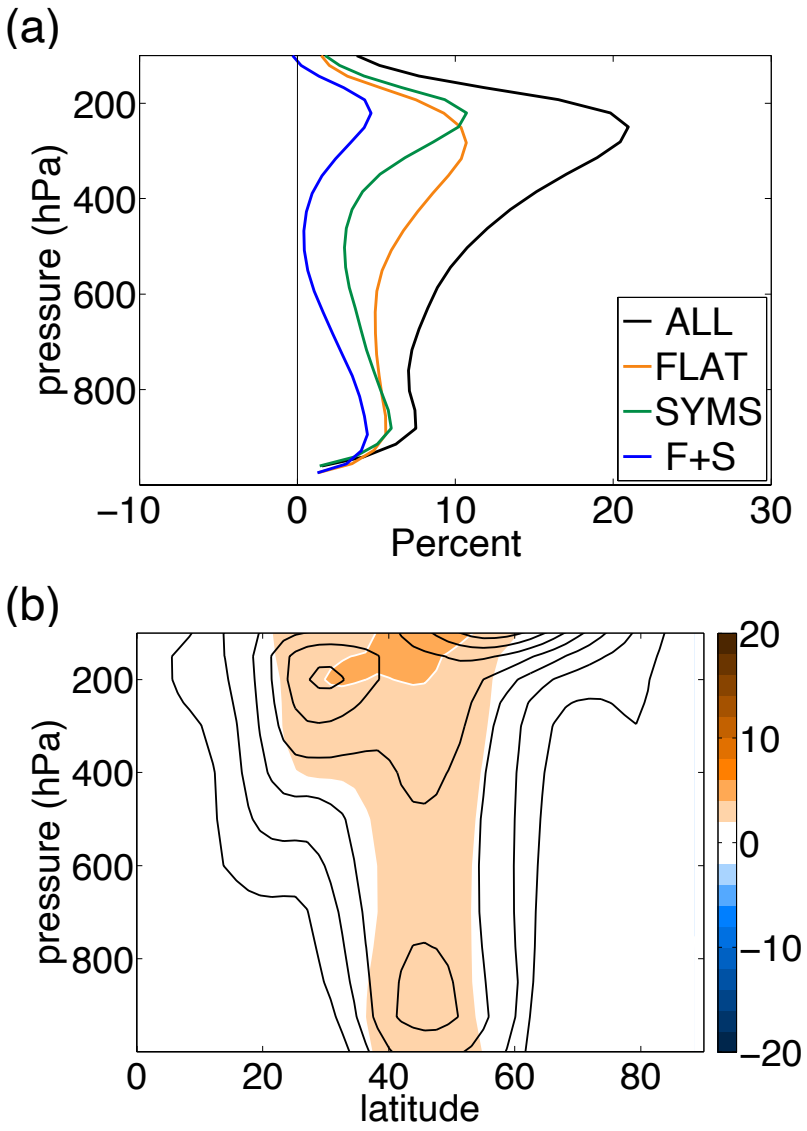

Fig. S4. Difference of Southern and Northern Hemisphere (a) storminess measured by vertically-varying transient eddy kinetic energy averaged poleward of 20° and divided by the value at 250 hPa in the Northern Hemisphere and (b) longitudinal-mean zonal wind (2.0 ms^{-1} contour interval) for ALL (black) and F+S (colors).

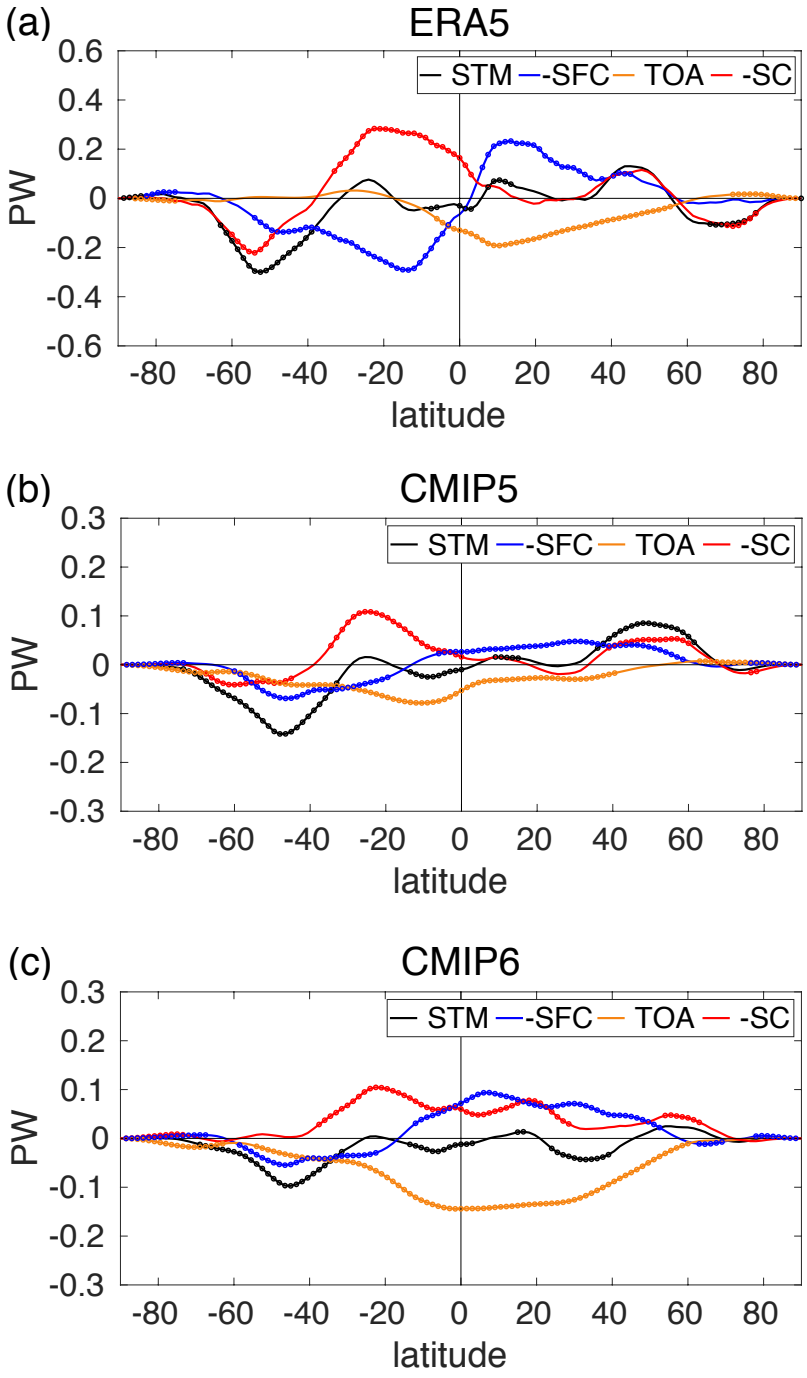

Fig. S5. Trend of eddy MSE flux storminess (STM) from 1980 to 2018 decomposed into contributions from surface energy fluxes (SFC), TOA radiative fluxes (TOA) and stationary atmospheric circulation energy fluxes (SC) in (a) ERA5 and for the (b) CMIP5 and (c) CMIP6 multi-model-mean. Trends that are statistically significant (p values smaller than 0.05) are marked with a circle.

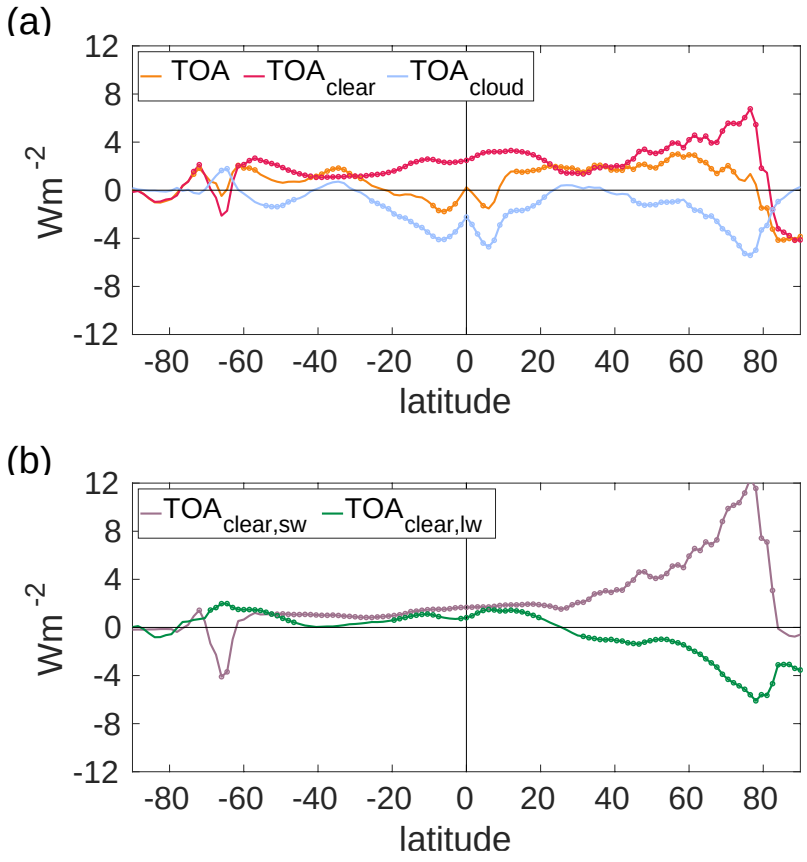

Fig. S6. (a) Trend of ERA5 TOA radiative fluxes from 1980 to 2018 decomposed into clear-sky and cloud-sky contributions. (b) Trend of ERA5 TOA clear-sky radiative fluxes from 1980 to 2018 decomposed into shortwave and longwave contributions. Trends that are statistically significant (p values smaller than 0.05) are marked with a circle.

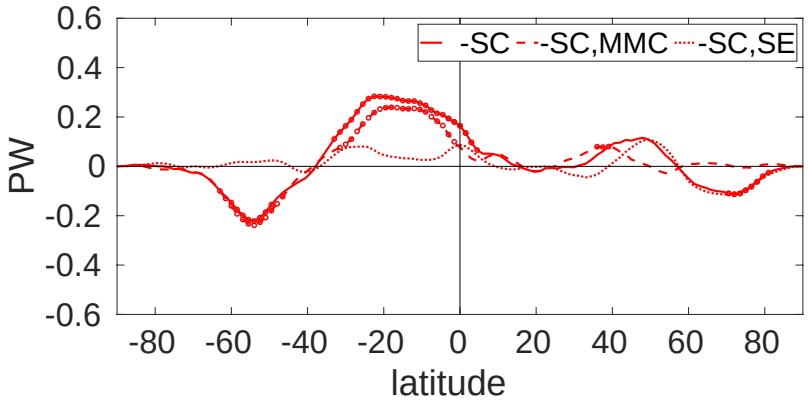

Fig. S7. Trend of ERA5 stationary atmospheric circulation energy fluxes (SC) decomposed into contributions from the mean meridional circulation (MMC, dashed) and stationary eddies (SE, dotted). Trends that are statistically significant (p values smaller than 0.05) are marked with a circle.

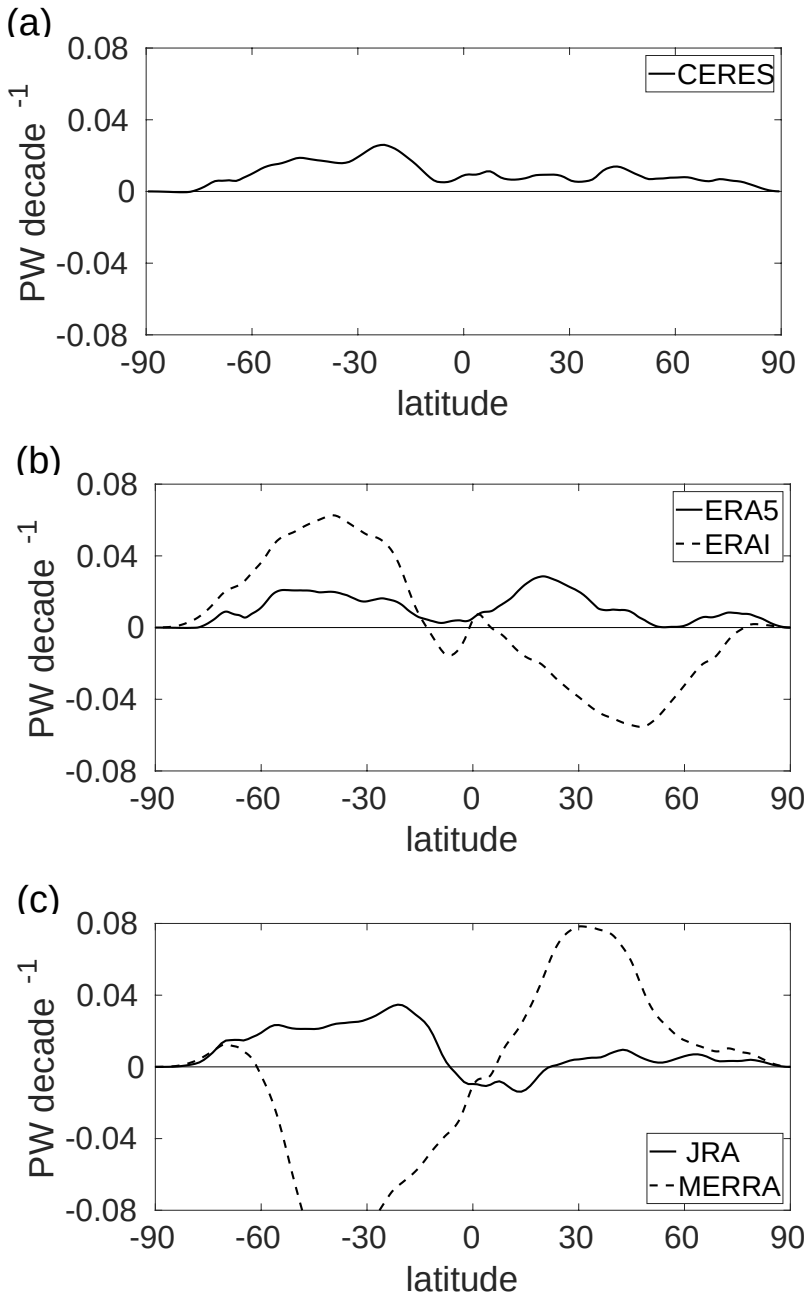

Fig. S8. Trend of energy flux implied from trends in TOA radiative energy fluxes from 2001 to 2018 for (a) CERES, (b) ERAI and ERA5, and (c) JRA55 and MERRA2 reanalysis data sets.

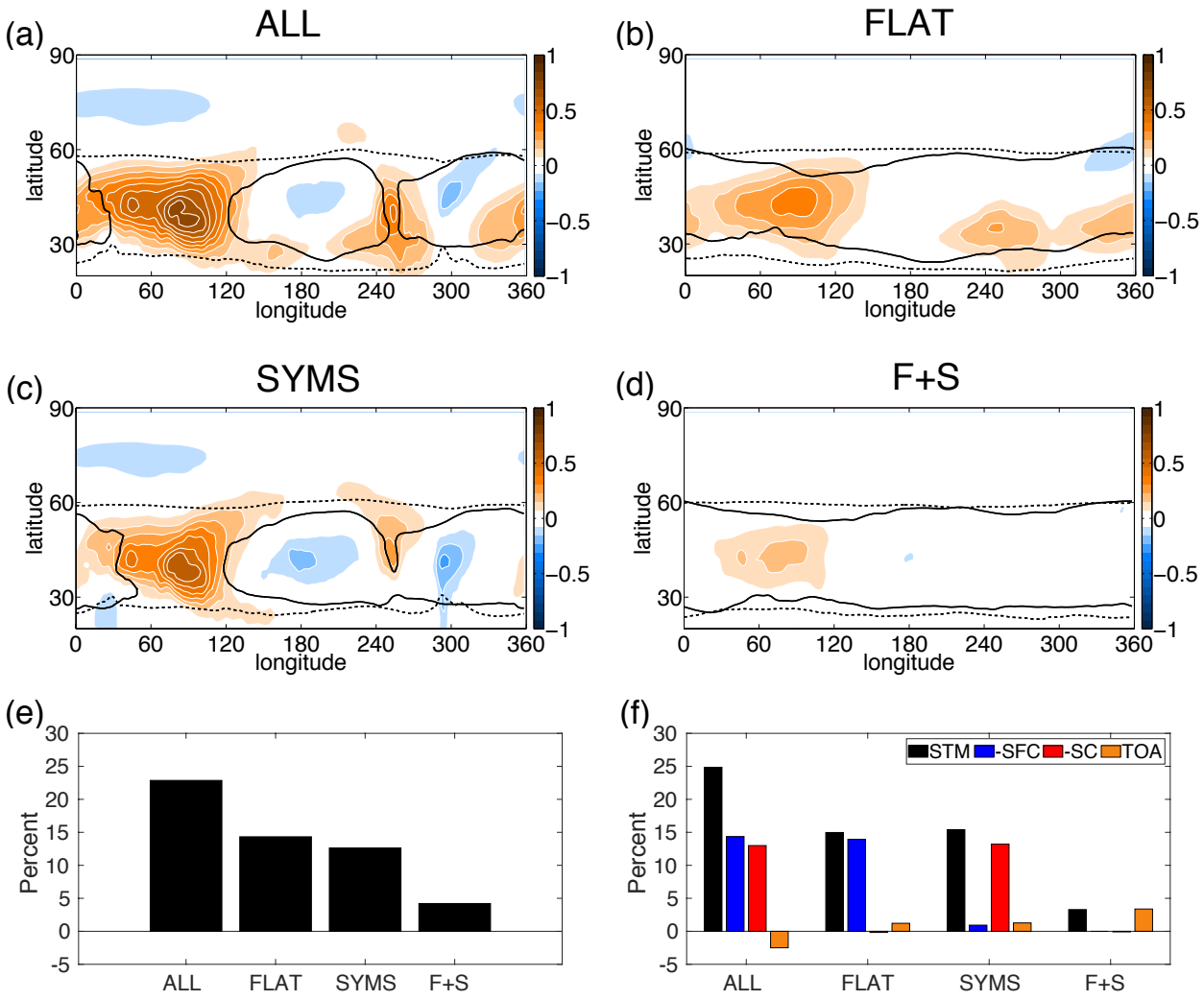

Fig. S9. Difference of Southern and Northern Hemisphere storminess (cosine-weighted vertically-integrated eddy kinetic energy, MJm^{-2}) in the climate model forced with qfluxes from an AMIP simulation for (a) climatology (ALL), (b) flattened topography (FLAT), (c) symmetrized surface energy fluxes (SYMS), and (d) flattened topography and symmetrized surface energy fluxes (F+S) simulations. The black lines in (a)-(d) indicate where storminess is equal to 0.6 MJm^{-2} for the Southern (dashed) and Northern (solid) hemispheres. Percentage difference of longitudinal-mean, vertically-integrated extratropical (poleward of 20°) storminess (difference of Southern and Northern Hemisphere divided by Northern Hemisphere) across the simulations for (e) eddy kinetic energy and (f) transient eddy moist static energy flux (STM) decomposed into surface energy flux (SFC), stationary circulation (SC) and top-of-atmosphere (TOA) contributions.

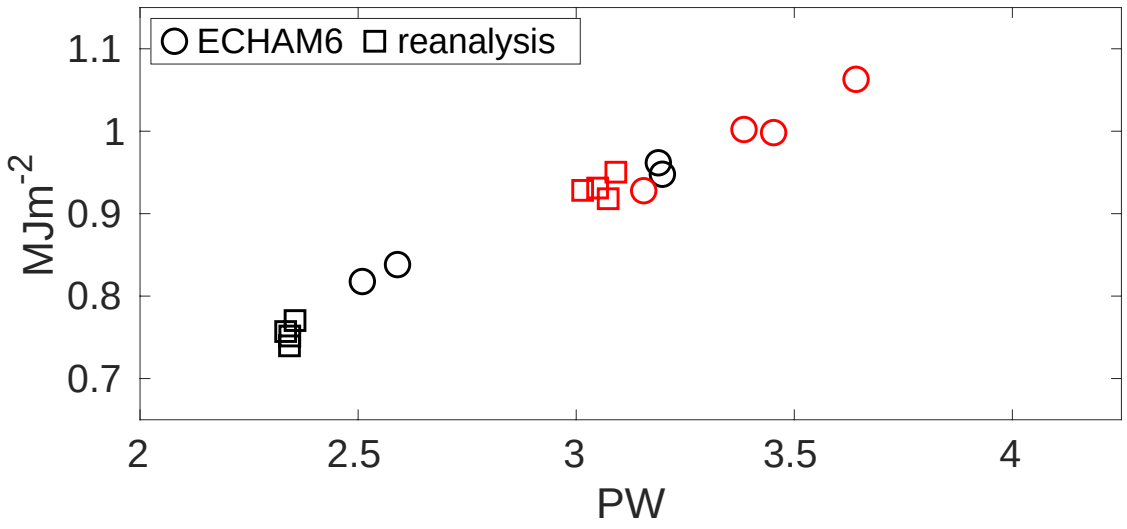

Fig. S10. Eddy kinetic energy versus transient eddy MSE flux for ECHAM6 simulations (circle) and reanalysis data (square) averaged over the extratropics (20-90°) of the Northern Hemisphere (black) and Southern Hemisphere (red).

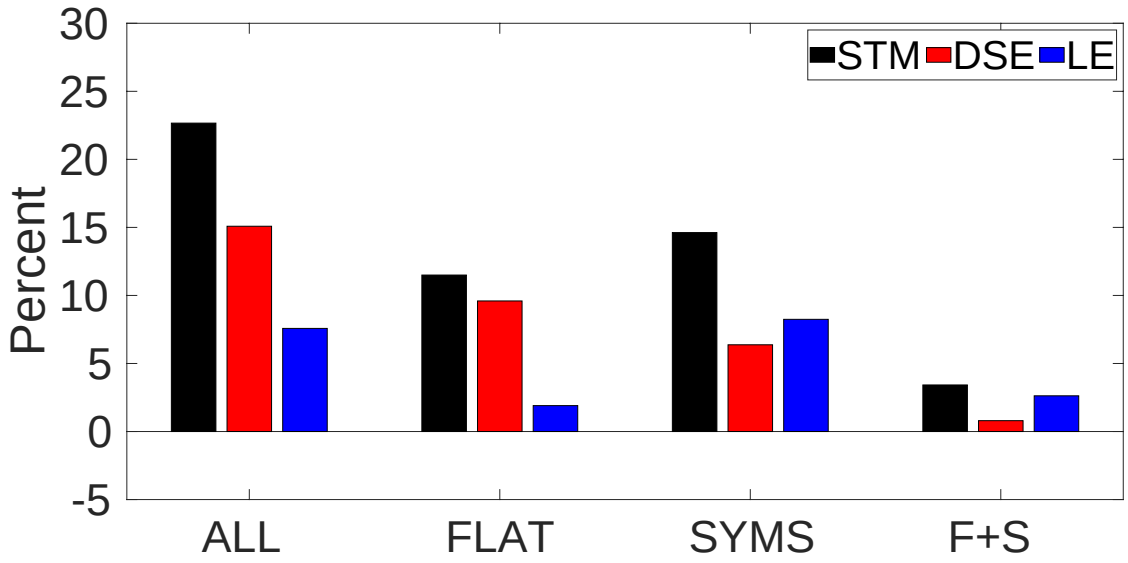

Fig. S11. Percentage difference of longitudinal-mean, vertically-integrated extratropical (poleward of 20°) energetic storminess (difference of Southern and Northern Hemisphere divided by Northern Hemisphere, STM black) across the simulations decomposed into dry static energy (DSE, red) and latent energy (LE, blue) contributions.

Table S1. Trends from 1980 to 2018 of Northern (NH, MJm^{-2}) and Southern (SH, MJm^{-2}) Hemisphere storminess and the Hemispheric asymmetry of storminess (ASYM, %) across reanalysis data sets and for the CMIP5 and CMIP6 multi-model mean. A star indicates trends where p value of the linear coefficient of the linear regression model is smaller than 0.05 (multi-model mean for CMIP) and brackets show the 10th and 90th percentile trend values across the CMIP model ensemble.

Data set	$EKE\,NH$		$EKE\,SH$		$EKE\,ASYM$	
ERAI	0.0036		0.0229*		2.7179*	
ERA5	0.0206		0.0421*		2.8390*	
JRA55	-0.0040		0.0293*		2.6964*	
MERRA2	-0.0025		0.0219*		2.3243*	
CMIP5	0.0043	(-0.0054,0.0070)	0.0109*	(-0.0008,0.0171)	1.0244*	(-1.2314,3.4438)
CMIP6	-0.0053	(-0.0223,0.0078)	0.0092*	(-0.0047,0.0187)	2.5073*	(-0.1682,6.1568)

Table S2. CMIP5 models analyzed in this study.

Model	*realization*
ACCESS1-3	r1i1p1
bcc-csm1-1	r1i1p1
bcc-csm1-1-m	r1i1p1
BNU-ESM	r1i1p1
CanESM2	r1i1p1
CCSM4	r1i1p1
CMCC-CESM	r1i1p1
CMCC-CM	r1i1p1
CMCC-CMS	r1i1p1
CNRM-CM5	r1i1p1
CSIRO-Mk3-6-0	r1i1p1
GFDL-CM3	r1i1p1
GFDL-ESM2G	r1i1p1
GFDL-ESM2M	r1i1p1
IPSL-CM5A-LR	r1i1p1
MIROC-ESM	r1i1p1
MIROC-ESM-CHEM	r1i1p1
MIROC5	r1i1p1
MPI-ESM-LR	r1i1p1
MPI-ESM-MR	r1i1p1
MRI-ESM1	r1i1p1
NorESM1-M	r1i1p1

Table S3. CMIP6 models analyzed in this study.

Model	*realization*
ACCESS-CM2	r1i1p1f1
CanESM5	r1i1p1f1
CESM2-WACCM	r1i1p1f1
EC-Earth3	r1i1p1f1
FGOALS-g3	r1i1p1f1
GFDL-CM4	r1i1p1f1
IITM-ESM	r1i1p1f1
INM-CM4-8	r1i1p1f1
INM-CM5-0	r1i1p1f1
IPSL-CM6A-LR	r1i1p1f1
KACE-1-0-G	r1i1p1f1
MIROC6	r1i1p1f1
MPI-ESM1-2-LR	r1i1p1f1
MPI-ESM1-2-HR	r1i1p1f1
MRI-ESM2-0	r1i1p1f1
NorESM2-LM	r1i1p1f1
NorESM2-MM	r1i1p1f1
TaiESM1	r1i1p1f1